American Mineralogist, Volume 92, pages 1936–1945, 2007

A modeling approach to understanding the role of microstructure development on crystal-size distributions and on recovering crystal-size distributions from thin slices

Roddy Amenta,* Anne Ewing, Amy Jensen, Sarah Roberts, Krista Stevens, Michelle Summa, Stephanie Weaver, and Paxton Wertz

Department of Geology and Environmental Science, James Madison University, Harrisonburg, Virginia 22807, U.S.A.

Abstract

Computer modeling of microstructure development was used to determine whether competition for space among growing crystals modifies the crystal-size distribution (CSD) predicted by the crystallization kinetics. Microstructures were modeled with prisms, plates, and cuboids, respectively. In all cases, the true CSDs calculated from crystal volumes in the microstructure corresponded closely with the linear ideal CSDs predicted by crystallization equations indicating that grain impingements did not significantly modify the predicted CSD information. Crystal intersection widths and lengths were measured in 2-dimensional slices through the microstructures to test if the CSD information could be recovered. For prisms and plates, the recovered CSDs compared favorably with the true CSDs, but cuboids yielded mixed results depending on their shapes and need further study. For prisms, the recovered CSDs were linear and for plates slightly curvilinear. These results indicate that rocks with recovered, curvilinear CSDs should be interpreted cautiously as indicators of complex crystallization histories, and that petrographic examination should have precedence in such interpretations.

Keyword: Crystal-size distribution, CSD, microstructure, computer modeling

Introduction

Crystal-size distribution (CSD) theory was developed by Randolf and Larson (1971) to quantify industrial crystallization processes. The theory was adapted to magma crystallization by Marsh (1988, 1998) and Cashman and Marsh (1988), and others have since used it to reconstruct kinetic and dynamic models of magma emplacement and crystallization (Armienti et al. 1994; Higgins 1998; Zieg and Marsh 2002; Mock et al. 2003; Bindeman 2003). Although the theory is now generally accepted, Pan (2001) argued that CSDs contain a bogus pattern unrelated to the crystallization kinetics [see responses by Schaeben et al. (2002) and Marsh (2002)]. Nevertheless, the need for validation of CSDs recovered from microstructures is critical to advance and draw reliable conclusions. A few studies have dealt with this need (Castro et al. 2003; Bindeman 2003; Gualda 2006; Mock and Jerram 2005). The present investigation addresses this need by comparing CSDs recovered from crystal intersection widths and lengths obtained in slices through microstructures with the true or actual CSDs calculated from the known crystal volumes.

Some of the early computer models simulated recrystallization in metals and ceramics graphically using small discrete area units (Anderson et al. 1986; Grest et al. 1986; Nasello and Ceppi 1986; Ohser and Muecklich 2000). More recent models have dealt with crystallization of igneous textures in both two and three dimensions. Elliott et al. (1997) measured dihedral angles between grains in slices to distinguish non-equilibrated textures, and Cheadle et al. (2004) measured porosity and permeability along grain boundaries to estimate the amount of trapped melt. Hershum and Marsh (2002) developed a 2-dimensional model using discrete area units to represent melt and solids and then compared textures formed by constant crystal growth and dispersive growth. Hershum and Marsh (2006) developed a 3-dimensional model in which Avrami crystallization controlled the timing of crystal nucleation and growth. Although their approach is fundamentally sound for continuous nucleation and growth processes, Avrami control appears to result in some timing problems between nucleation and growth when they are modeled in discrete time stages. Amenta (2001) and Amenta et al. (1992, 1997a, 1997b, 2002) developed 2- and 3-dimentional models in which crystals grew using their own internal lattice patterns as distinct from the voxel method of representing portions of crystals. The latter model, with recent modifications that incorporate crystal nucleation and growth laws, was used in the present investigation.

Crystal sizes measured from slices must be corrected for the intersection probability effect and the cut-section effect (Underwood 1970). Corrections for the former are simple for spheres (Royet 1991), and correction schemes have been developed for other shapes (Saltikov 1967; Royet 1991; Peterson 1996; Sahagian and Proussevitch 1998). Corrections schemes for the latter are complex and highly dependent on crystal shapes (Saltikov 1967; Sahagian and Proussevitch 1998; Higgins 1994, 2000). Both corrections are incorporated in the program CSDCorrections (Higgins 2000), which was tested on tetragonal prisms and plates but apparently not on cuboids (rectangular parallelepipeds that have three unequal axes). The primary recovery method used in the present investigation is CSDCorrections and the secondary method for comparison is that of Underwood (1970) and Marsh (1988) that corrects only for the intersection probability effect.

Several studies have tried to identify the measurable param-

* E-mail: amentarv@jmu.edu

0003-004X/07/1112–1936$05.00/DOI: 10.2138/am.2007.2408

eters of crystals in thin section that are the most reliable indicators of crystal sizes (Chayes 1950; Higgins 1994; Peterson 1996; Sahagian and Proussevitch 1998). Higgins and Peterson found that the intersection width best represents the short dimension of tetragonal prisms and intersection length the intermediate (=long) dimension of tetragonal plates. Peterson found that sizes of cuboids could not be reliable determined from slices, yet Higgins suggested that the intersection length is the best indicator for the intermediate dimensions of cuboids. The present study will try to clarify this. There is yet no clear choice between using direct measurements of intersection widths and lengths vs. the major and minor diameters of ellipses. It is probably more important to be consistent using the same method when comparing CSDs recovered from thin sections. In the present study, ellipse diameters (as opposed to radii) were used as indicators of crystal size, and for consistency, the term "diameter" rather than "dimension" was used in all the CSD charts. The first part of the study deals with computer modeling of crystallization with development of microstructures. The second part deals with assessing the recovering of CSD information from 2-dimensional slices through the microstructures.

Modeling crystallization

The computer model used in this analysis has been described in detail (Amenta et al. 1997a, 1997b; Amenta 2001). We comment here on the modifications to this model that relate to crystal nucleation and growth. A critical part of any crystallization algorithm is the method chosen to measure a crystallization time-step since computer time obviously is not such a measure. Hersum and Marsh (2002, 2006) related time to the percent crystallization as predicted by an Avrami function. To better synchronize nucleation and growth, we did not use an Avrami function but linked a time-step unit directly to a growth stage, the span in which all crystals have grown by a constant increment in diameter, ΔL. Thus nucleation occurred in a burst at the beginning of each growth stage or time step. Crystal nuclei were located and oriented randomly in the available unoccupied space, and crystals did not move once they were positioned. Time-steps units were dimensionless and consisted of a sequence of integer numbers (i.e., 1,2,3...n).

Each crystal was assigned a reserve quota of unit cells that were drawn upon for the crystal to achieve its new diameter. Each quota was calculated on the basis of the expected volume increase of that crystal. All crystals began to draw on their quotas at the beginning of the growth stage. A growth stage had several iterations in which a unit cell was added to each crystal in the population in a sequential fashion. Thus, unit cells were added to each crystal at the same rate ensuring that both large and small crystals competed equitably for space. Iterations were repeated until all crystals had either exhausted their quotas, or had become inactive due to impingements. A crystal became inactive when a unit-cell vacancy in the crystal lattice could not be found after a large number of failed search attempts. Small crystals had fewer cells in their quotas than large crystals, so the small crystals finished growth earlier in a growth stage than the larger ones. Each crystal lattice was cubic with a unit-cell spacing of 0.4 mm (unit-cell volume of 0.064 mm^3). This spacing was chosen because it optimized the resolution of individual crystals by their pixel patterns in the microstructure. Smaller spacing decreased resolution and incurred longer computer run times. Crystals that grew and impinged against the boundaries of the chamber obeyed the same rules as if impinging against other crystal boundaries, i.e., their unit cells were located elsewhere within their lattices, thus the volumes and sizes of these boundary crystals would be as predicted by their quotas. The crystallization chamber was setup as a cube subdivided into $100 \times 100 \times 100$ mm^3 integer volume units. The unit cells were mapped into these volume units on a first-come basis (Amenta 2001). Each crystallization run produced a primary database of unit cells joined to crystals in relative time order, and each cell was identified with a specific crystal to which it was attached. This database was used to determine the volumes and sizes of the crystals as explained below.

Many rocks contain linear or nearly linear CSDs (Higgins 2006), and the assumption of linearity is often a first approximation in their analysis. Linear CSDs were modeled in the present study with an algorithm in which all crystals grow by a constant diameter increment with each time step coupled with a nucleation rate that increases exponentially with time. The following discrete equations predict ideal crystal sizes and their CSDs without regard to unit cells making up the crystals. The bin width was determined by Equation 1, and the number of crystals (all equal in size) in each bin determined by Equations 3 and 5.

$$\Delta L = \text{constant} \quad (1)$$
$$\Delta t = 1 \quad (2)$$
$$t = 0,1,2,3...t_c \quad (3)$$
$$G = \Delta L/\Delta t = \text{constant} \quad (4)$$
$$N_t = e^{(at)}. \quad (5)$$

ΔL is the change in a crystal short diameter at the end of each growth stage and time-step unit, Δt, and G is the crystal growth rate constant. The clock that counted the number of growth stages is t, and the characteristic crystallization time that marked the effective end of crystallization is t_c. N_t is the number of new nuclei formed at each time step, and the exponential nucleation constant is a. Values of ΔL were restricted to 0.20 mm, and a to values less than 1.0/t. These values ensured that N_t did not grow too large and dominate crystallization, that there were a sufficiently large number of nucleation events (30 to 40) to define the CSDs, and that the resolution problem in the measurement of very small crystal sizes was minimized. To ensure linearity in the CSDs, the nucleation rates were not based on the amount of melt remaining in the chamber (Marsh 1998). Instead, the chamber was open with respect to the melt, but closed with respect to crystallization.

In a log-linear CSD plot, the slope is negative because the crystal sizes increase with time as their numbers decrease. The slope of a CSD resulting from applying Equations 1, 2, and 3 can be determined by differentiation and is equal to the ratio of the nucleation constant, a, and crystal growth rate constant, G, as shown in Equations 6 and 7

$$d[\ln(N_t)]/dL = (-)d\,[\ln e^{(at)}]/d\,(Gt) \quad (6)$$
$$(-)d\,[\ln e^{(at)}]/d\,(Gt) = (-)a/G. \quad (7)$$

The ideal short diameters, S_{ideal}, of the crystals in each bin were calculated by Equation 8,

$$S_{ideal} = (t)(\Delta L) \quad (8)$$

where t is the growth time for the crystals in that bin size. Note that the population density Equation 9 has a form similar to Equations 6 and 7,

$$d\ln(n)/dL = (-)a/G \quad (9)$$

where n is the population density, i.e., the number of crystals/bin width/system volume or $1/mm^4$.

It should be noted that a more frequently cited equation of the slope of a log-linear CSD is Equation 2 in Marsh (1998) and restated below as Equation 10 where τ is the average residence time for crystals moving in and out of a dynamic crystallization system at steady state:

$$d\ln(n)/dL = 1/G\tau. \quad (10)$$

In closed, non-steady state systems, as in the present study, the average residence time has a different meaning and Equation 9 does not strictly hold.

Validating the results of the crystallization model

Qualitative and quantitative methods were used to validate that the crystallization model generated microstructures and CSDs consistent with the experimental control parameters. The similar appearances of grain sizes and shapes in three perpendicular slices through the chamber suggested that the microstructures were uniform in three dimensions. In many slices the final available spaces became localized in pockets (Fig. 1a) rather than uniformly distributed, and that the latest nuclei or smaller crystals tended to be located in these pockets. Despite the modifications of crystal shapes by their impingements against other crystals, their basic shapes were still discernible from the shapes of their intersection polygons in the slices (Higgins 1994,

2000). For example, slices through microstructures composed of tetragonal prisms revealed numerous, irregular, square-shaped polygons that reflect the abundance of short and intermediate crystal diameters (Fig. 1a), and slices through microstructure composed of tetragonal plates revealed numerous, irregular, blade-shaped polygons that reflect the abundance of intermediate and long crystal diameters (Fig. 1b).

Using a numerical validation approach, we next determined how the true numbers of crystals in each bin size compared to the ideal numbers predicted by the model. These numbers are extensive parameters related to the size of the chamber, and they serve to relate the actual numbers of crystals grown relative to the chamber volume. We will designate them as the true population CSD and the ideal population CSD, respectively, in contrast to their population density CSDs to be discussed later. An ideal crystal size is a pure geometric measure as predicted by Equation 8.

The actual long diameters of crystals could not be measured directly due to algorithmic problems. Some of the larger crystals had outliers of unit cells that extended beyond their host crystals causing errors in their length calculations. Instead, the true volume of a crystal, $V_{true,}$ was calculated by multiplying the unit-cell volume by the number of cells, c, in the crystal (Eq. 11)

$$V_{true} = c(0.064)\text{mm}^3. \qquad (11)$$

Since Figures 1a and 1b suggest that crystal shapes and axial ratios have not changed significantly by their impingements, the crystal volume can be related to its axial ratios expressed as (1:j:k) (short:intermediate:long) in Equation 12

$$V_{true} = S_{true}\,(1)\,S_{true}\,(j)\,S_{true}\,(k)\ \text{mm}^3. \qquad (12)$$

Combining Equations 11 and 12 and solving for the true short diameter gives

$$S_{true} = \sqrt[3]{\frac{c(0.064)}{(j)(k)}}\ \text{mm}. \qquad (13)$$

Equation 13 gives the program output in terms of true short diameters, which is analogous to Equation 8, which gives the program input in terms of ideal short diameters. The long diameters, however, were used as the measure of crystal sizes in all the CSD plots to be consistent with the CSD results of CSDCorrections. The long diameters were calculated by multiplying S_{true} and S_{ideal} by k. It should be noted that the long diameters could be calculated directly by expressing the axial ratios as i:j:1, but the results are the same.

The true population and ideal population CSDs for seven microstructures, each composed of unique crystal shapes are shown in Figure 2. Overall the ideal population CSDs showed almost straight alignment of data points (excluding the few larger crystals) as predicted by Equation 7. The true population CSDs, as expected, showed more scattering of points especially in the larger and smaller bins sizes. The scatter is probably caused by several factors including the effects of crystal impingements on crystal growth, the growth of batches of crystals in discrete stages rather than in a continuous manner, the paucity of large crystals, and the high sensitivity of the smallest crystals to large percentage changes in their volumes. Most of this scatter appears to be random and non-systematic as shown in data sets of prisms 1:1:5 (Fig. 2a), plates 1:3:3 (Fig. 2d), and cuboids 1:2:5 (Fig. 2g); and in these there is very close agreement between the slopes of the true CSDs and their respective ideal CSDs. This scatter could be explained by grain impingements that would cause the populations in certain bins to decrease and those of adjacent bins to increase. However, the CSDs of prisms 1:1:3 (Fig. 2b), plates

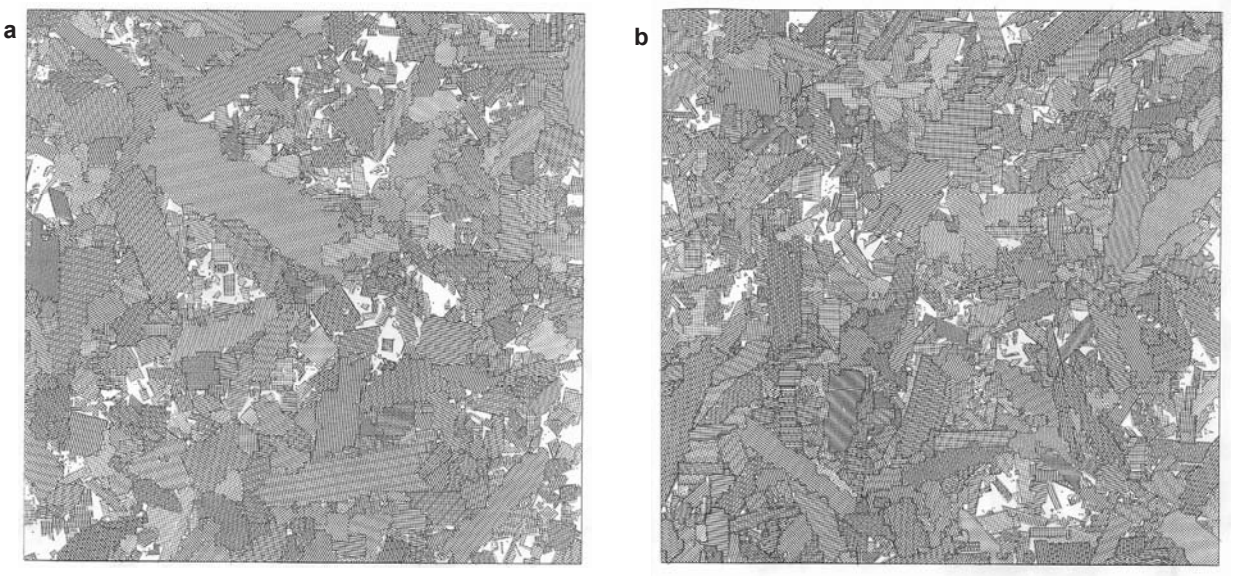

FIGURE 1. Examples of microstructures viewed in digital slices cut through the crystallization chamber. The chamber is $100 \times 100 \times 100$ mm^3, and the slice dimensions are 100×100 mm^2. CSDs were recovered from measurements of 2-dimensional crystals sizes from such slices. (**a**) Slice shows microstructure composed of prism-shaped crystals with dimensional ratios 1:1:5. Crystal boundaries have been outlined by hand. Note abundance of square sections. (**b**) Slice shows microstructure composed of plate-shaped crystals with dimensional ratios 1:5:5. Crystal boundaries have been outlined by hand. Note abundance of blade-like sections.

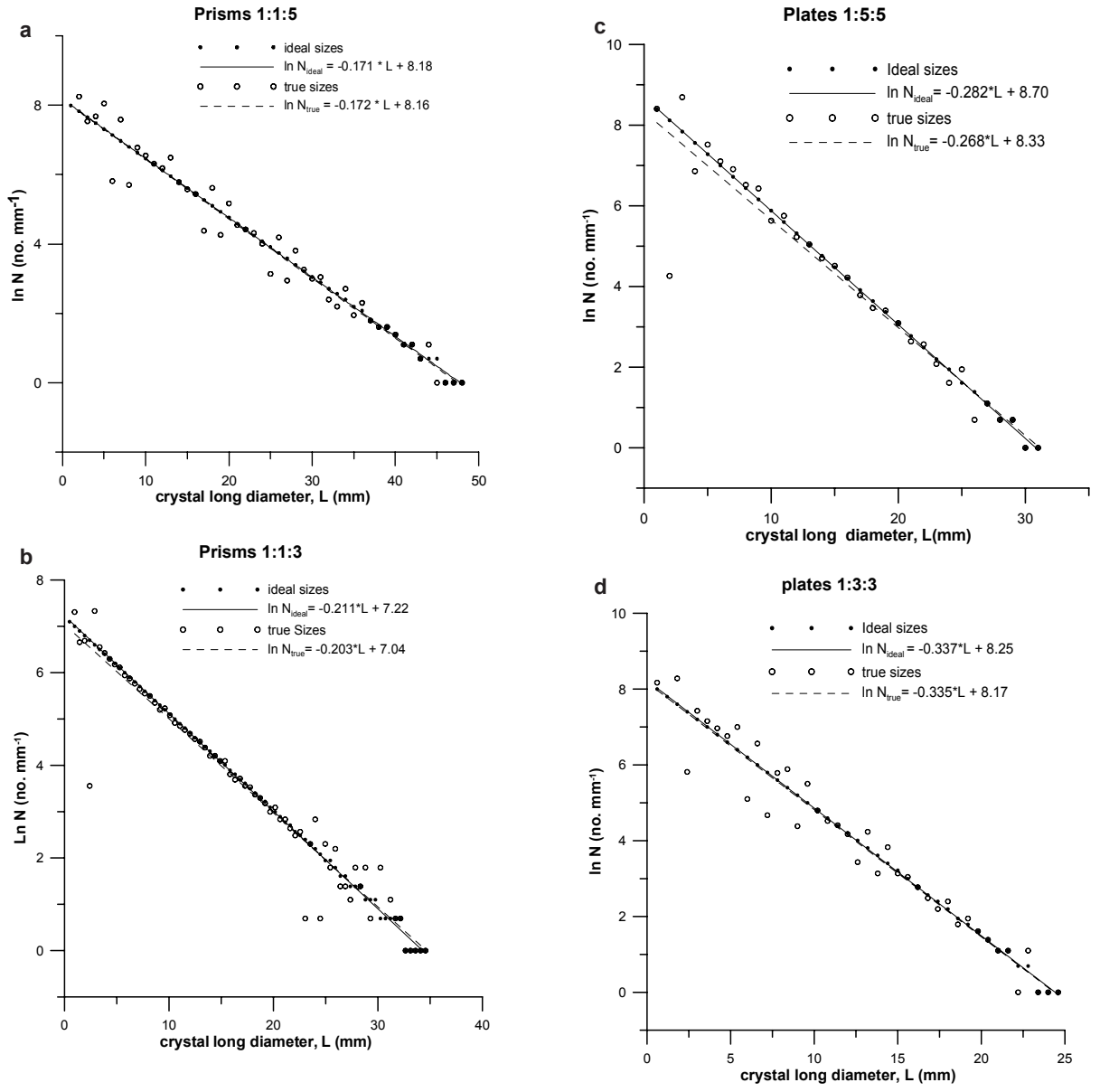

Figure 2. These charts, and Table 1, serve to validate the results of the forward crystallization model by comparing the true numbers of crystals in each bin size (dashed line and open circles) with the ideal numbers (solid line and solid dots). The ideal numbers are determined by the nucleation function (Eq. 5) at the beginning of each discreet time step. The scatter in the true numbers vs. their bin sizes show the modifying affects of the microstructure on grain growth, yet despite this scatter (see R^2 values for true CSDs below), the best-fit regression lines for the true CSDs are in close agreement with the ideal CSDs. (**a**) prisms 1:1:5, $R^2 = 0.9677$; (**b**) prisms 1:1:3, $R^2 = 0.9375$; (**c**) plates 1:5:5, $R^2 = 0.9163$; (**d**) plates 1:3:3, $R^2 = 0.9579$; *continued next page.*

1:5:5 (Fig. 2c), cuboids 1:3:5 (Fig. 2f), and cuboids 1:4:5 (Fig. 2e) also each contained an anomalous low point in the small bin sizes. These anomalies appear to be similar systematic errors incurred in calculating crystal volumes based on the number of contained unit cells. A unit cell comprises a large percentage of the volume of a small crystal, and the presence or absence of a cell can change the bin size of the crystal. Although the anomalies produced small biases in the CSD slopes, we included the points in the regressions because we did not want to alter the CSD information in the primary data sets. Values of the coefficient of determination (R^2) for the true CSDs are given in the captions of Figure 2. Overall, the slopes of the true CSDs are close to their respective ideal ones. The percent slope deviation is +0.584% for the prisms 1:1:5; –3.79% for prisms 1:1:3; –4.96% for plates 1:5:5; –0.593% for plates 1:3:3; –3.56% for cuboids 1:4:5; –6.23% for cuboids 1:3:5; and +1.49 for cuboids 1:2:5. A negative percent difference indicates that the true CSD slope was less than the ideal CSD slope. The higher negative deviations are caused by the anomalous low points referred to above and not by the microstructure, so if the low points had been excluded then all deviations would probably have been less that 1.5%. These results suggest that the microstructures appear to

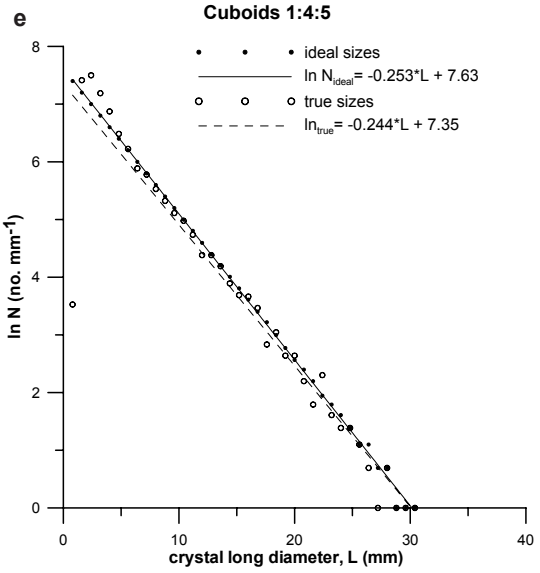

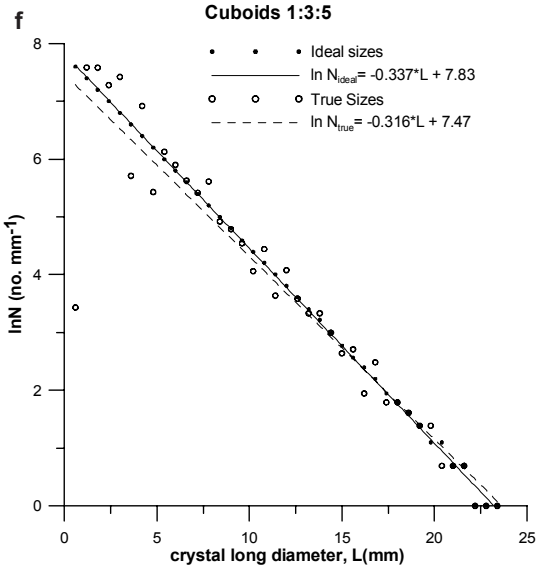

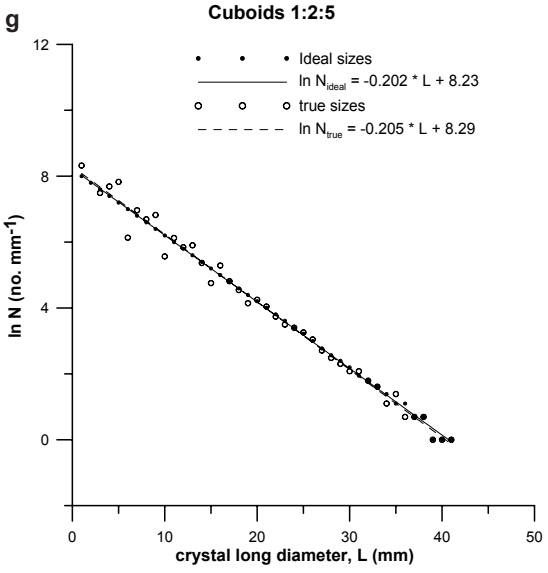

FIGURE 2.—*Continued:* (**e**) cuboids 1:4:5, $R^2 = 0.9156$; (**f**) cuboids 1:3:5, $R^2 = 0.8992$; and (**g**) cuboids 1:2:5, $R^2 = 0.98798$.

retain the original CSD information despite some modification of crystal shapes by grain-to-grain impingements. These results also helped to validate that the crystals that have grown into the chamber boundaries are the correct sizes as would be expected by their assigned volume quotas of unit cells.

To evaluate the spatial efficiency of the crystallization model, all of the crystals in the chamber were used to compare the total true volume of crystals with the total ideal volume of crystals and the volume of the chamber. Most of the crystallization experiments required about 25 days of PC computer time to reach 98% crystallization as measured by the number of integer volume units in the chamber occupied by crystals. Additional time produced very little increases in crystallization. However, a better measure of the percent crystallization achieved is based on the summation of the unit-cell volumes for each crystal in the chamber using Equation 11. By this measure, the total true volumes of crystals range from 85 to 97% of the chamber (Table 1). It is interesting to compare this range with the total ideal volumes of crystals (Table 1) that range from 91 to 111% (note that the ideal sizes of crystals are not constrained by impingements, and their total volume can exceed the size of the chamber). The total ideal volumes of crystals is based on a summation of all the ideal crystal volumes using an equation similar to Equation 12. The total true volumes are 6 to 14% smaller because this reflects the constrained growth of the true crystals in the microstructure. The volume difference may be viewed as that associated with grain boundaries caused by misfits of the crystal lattices along grain boundaries. However, the grain boundary volumes in our microstructures depend on the arbitrary unit-cell spacing of 0.04 mm used in this study and should not be extrapolated to grain boundary volumes and porosities in rocks.

RECOVERING CSD INFORMATION FROM THIN SLICES

In the previous section, we demonstrated that a computer model generates microstructures containing true CSDs that are close to the ideal ones predicted by the crystallization kinetics. We will now evaluate how well the known true CSDs can be recovered from 2-dimensional slices through the microstructure using the program CSDCorrections (Higgins 2000) version 1.36, and the method of Underwood (1970). A 2-dimensional slice through the chamber is obtained by sorting the database for all unit cells in a given plane. For example, if the Z dimension of the chamber ranges from 0 to 100 mm, a plane perpendicular to Z that has a finite thickness from Z = 50 to Z = 51 would contain all cells with coordinates (X,Y,50.0–51.0). When these cells are plotted graphically, each crystal assumes a distinct pixel pattern due to the slice angle through its lattice. The resulting image resembles that of a thin section 100 × 100 mm^2 (Figs. 1a and 1b). To facilitate measuring crystal outlines, small subsets of widely separated crystals were selected from the slice (Fig. 3). Each crystal outline was traced by hand using image analysis software, and the major and minor axes of its approximating ellipse were determined. We shall use these axes as representations of the intersection length

TABLE 1. Parameters from seven computer runs serve to validate the performance of the forward crystallization model

(1) Data set identify-cation	(2) Number of crystals in chamber size of 100^3 (mm^3)	(3) True volume of crystals (mm^3)	(4) Ideal volume of crystals (mm^3)	(5) Number of crystals measured in 2D slices	(6) Number of crystals less crystals on boundaries	(7) Intersection width/length. S, I, or *L* crystal dimension
Prisms (a) 1:1:5	18 869	914 005	966 057	1386	1216	width, S
Prisms (b) 1:1:3	11 509	853 394	910 590	1543	1340	width, S
Plates (c) 1:5:5	18 203	979 694	1 114 570	2301	2017	length, *L*
Plates (d) 1:3:3	16 438	900 564	944 237	2044	1825	length, *L*
Cuboids (e) 1:4:5	9018	958 381	1 128 585	1298	1097	length, I
Cuboids (f) 1:3:5	11 016	962 449	1 041 728	1644	1423	length, I
Cuboids (g) 1:2:5	16 438	914 045	966 057	1973	1710	width?, I

Notes: Column 1 identifies the crystal shape ratios used in each experiment. Column 2 contains the total number of crystals grown in each experiment in a chamber size $100 \times 100 \times 100$ mm^3. Column 3 shows the true or actual volume of crystals grown in the chamber. Column 4 shows the ideal volume of the same crystals if they had been able to grow in free space with ideal sizes and shapes. Note that the ideal volumes in the three data sets—c, e, and f—exceed the size of the chamber. Column 5 shows the total number of crystals measured in two or three orthogonal slices through the chamber. Column 6 shows the number of crystals in the subset that do not touch the boundaries of the slices. Column 7 identifies the crystal's intersection width or length as the best indicator of the crystal's small diameter (S), intermediate diameter (I), or long diameter (*L*).

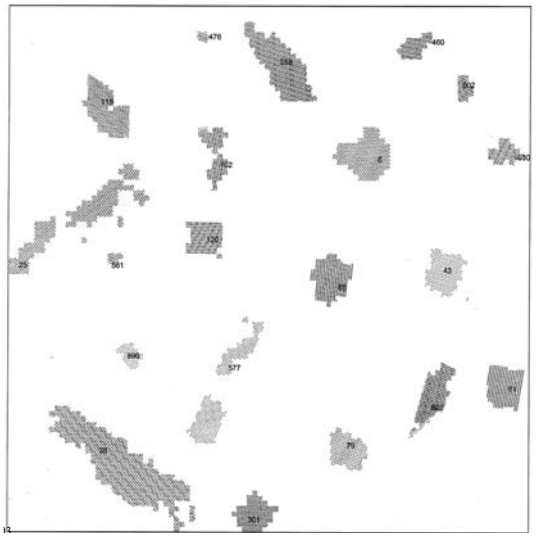

FIGURE 3. Slices that contain subsets of crystals allow crystal boundaries to be easily traced as shown in this subset of prisms (1:1:5). Identification numbers relate to the order in which the crystals nucleated. Note that host crystals 25 and 577 appear to have detached outliers, but the outliers are actually connected to their hosts in 3 dimensions.

and width, respectively.

Between 1300 and 2300 crystals were measured in each experiment (Table 1) depending on the average grain size of the microstructure, which required three mutually perpendicular slices taken through the center of the chamber. Crystals touching the slice boundaries were included in the CSD analyses that follow, and the reason for doing so is described later. Some crystals had outliers (Fig. 3), which appeared to be detached from the host, but tests using parallel serial slices revealed that the outliers were connected to their hosts in 3-dimension. The areas of the outliers were included within the outline traces of their hosts to account for the entire surface area of each crystal in the slice. In each data set, we tested both the intersection lengths and widths as indicators of crystal sizes. Our findings confirm those of Higgins (1994) and Peterson (1996) that the intersection widths best correlate with the short diameters of tetragonal prisms and intersection lengths with the intermediate diameters of tetragonal plates. With cuboids in general, the choice of the best indicator of crystal size remains a problem. Higgins (1994) reported that the intersection length was the best indicator of crystal size. Our findings, however, suggested that this is true only for a subclass in which the intermediate diameter approaches the long diameter. This subclass will be discussed later.

Crystal sizes were measured in slices through the seven microstructures, and these data sets are summarized in Table 1. The intersection length or width that is the best measure of crystal size is indicated, but it should be noted that in all graphs, crystals sizes are recast as long diameters regardless of the intersection distance measured. The CSDs recovered from the slices are shown in the graphs of Figures 4a–4g. In each graph, the true CSD is compared to that recovered using the primary method of CSDCorrections and the secondary method of Underwood. We determined the best-fit, linear-regression lines for the results of CSDCorrections to compare their slopes and intercept values with the corresponding true sizes CSD. Higgins (2000) recommended using a grouping of 5 $\log_{10}$ bins per decade with continuously variable crystal sizes. We explored various bin size groupings because our synthetic data were in discrete size groupings. Optimum results were obtained using 6 $\log_{10}$ bins per decade, which resulted in approximately 10 bins of unequal width with the largest width containing the largest crystals sizes. This minimized the scatter of points due to the paucity of large crystals, but may account for the scatter of points in the smallest sizes. We used the Underwood method (1970) as a secondary method but the bin widths were doubled ($2\Delta L$) to reduce scatter. The Underwood method was useful for identifying whether the intersection width or length was the best measure for crystal size, and it yielded sizes for the largest crystals that better matched the true and ideal crystal sizes.

In general, CSDCorrections yielded the best approximations to the linear slopes and vertical intercept values of the true crystal sizes CSDs (Fig. 4). The Underwood method yielded more strongly curvilinear, concave upward, CSDs especially in the range of the smaller crystal sizes, and these data were fitted to a linear regression line. Peterson (1996) showed similar curvilinear trends for CSDs recovered from his synthetic linear data sets although he used different stereological correction methods. Peterson (1996) suggested that, because the largest crystals are too few in number and the smallest crystals have measurement resolution problems, only the intermediate bin sizes by used in the regression analyses for the CSD. We also found that the intermediate bin sizes in our data sets, were better behaved than the largest and smallest bin sizes. For example, in some data sets CSDCorrections yielded crystal sizes that were anomalously

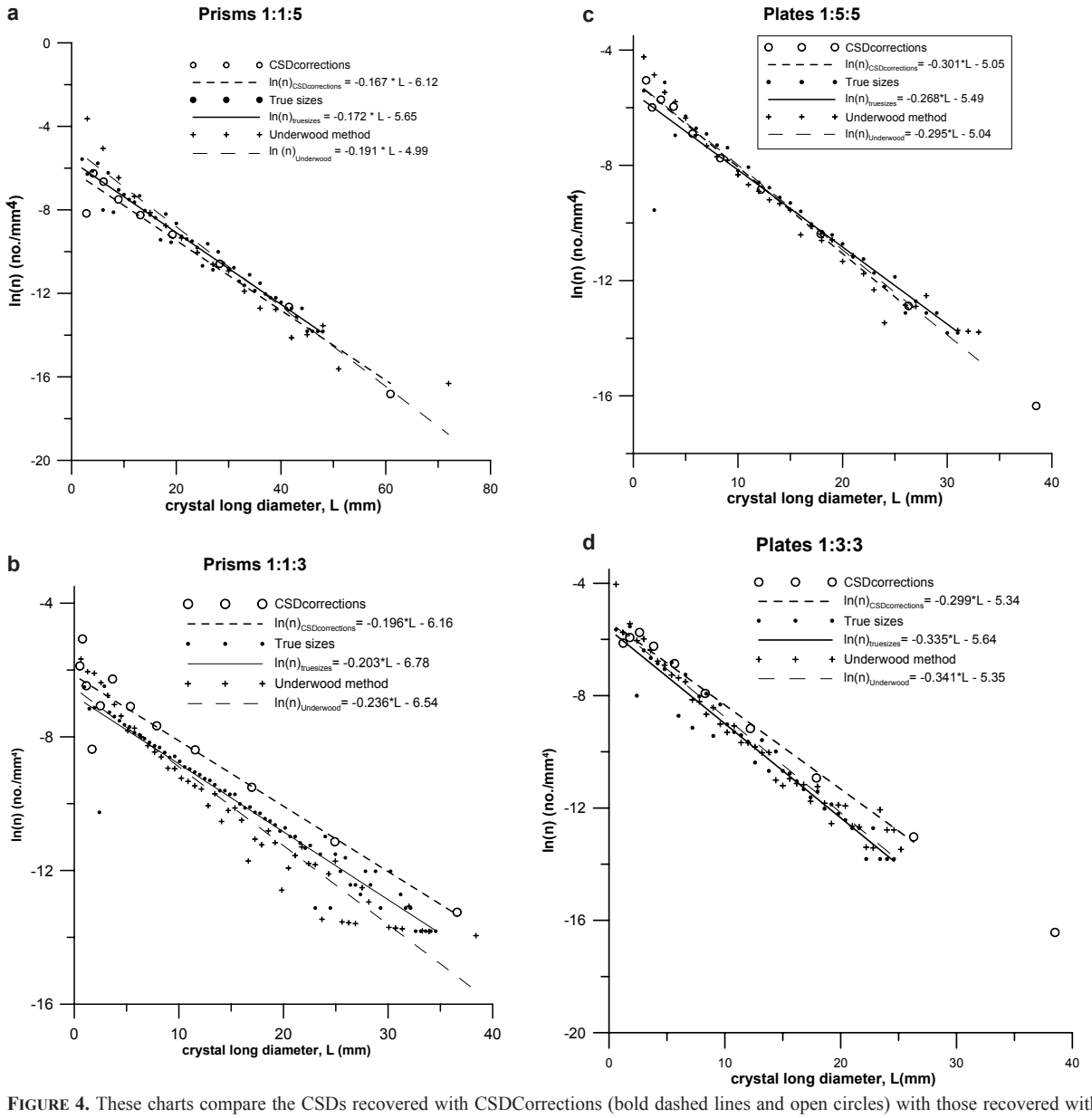

Figure 4. These charts compare the CSDs recovered with CSDCorrections (bold dashed lines and open circles) with those recovered with the Underwood method (thin dashed lines and crosses) with the CSDs of the true crystal sizes (solid lines and dots). The Underwood method consistently produced more pronounced curvilinear CSDs. The CSDs from CSDCorrections yielded the best overall approximations of linearity, slope, and intercept values. The R^2 and r_s values for CSDCorrections are listed below. (**a**) prisms 1:1:5, $R^2 = 0.960$ and $r_s = –0.996$; (**b**) prisms 1:1:3, $R^2 = 0.903$ and $r_s = –0.867$; (**c**) plates 1:5:5, $R^2 = 0.991$ and $r_s = –0.964$; (**d**) plates 1:3:3, $R^2 = 0.990$ and $r_s = –0.952$; (**e**) cuboids 1:4:5, $R^2 = 0.976$ and $r_s = –0.964$; and (**f**) cuboids 1:3:5, $R^2 = 0.951$ and $r_s = –0.820$; CSDCorrections yielded less satisfactory CSD approximations for (**g**) cuboids 1:2:5, $R^2 = 0.740$ and $r_s = –0.762$ but results were better than those of the Underwood method.

larger than those yielded by the Underwood method and those in the true sizes (Figs. 4c, 4d, and 4f). This discrepancy could not be due to our use of axes of ellipses as measures of intersection distances because this convention was also used in the Underwood method. Therefore, we did not include the anomalous points in the regressions although we showed them in Figures 4d, 4c, and 4f. The points for the smallest crystal sizes showed the most scatter, but we included them in the regressions because the scatter appears to be random.

CSDCorrections gave the best overall agreement between the recovered CSDs and the true sizes CSDs especially in the prisms. The data sets in which the recovered CSDs most closely approximate the true CSDs are shown in the first six charts in Figure 4. In the prisms 1:1:5 (Fig. 4a) and 1:1:3 (Fig. 4b), CSDCorrections yielded linear trends of points with very good agreement in their CSD slopes with those of the true sizes CSDs. In the prisms 1:1:3, a higher vertical intercept (nucleation density when crystal size, L, approaches zero) translated into slightly

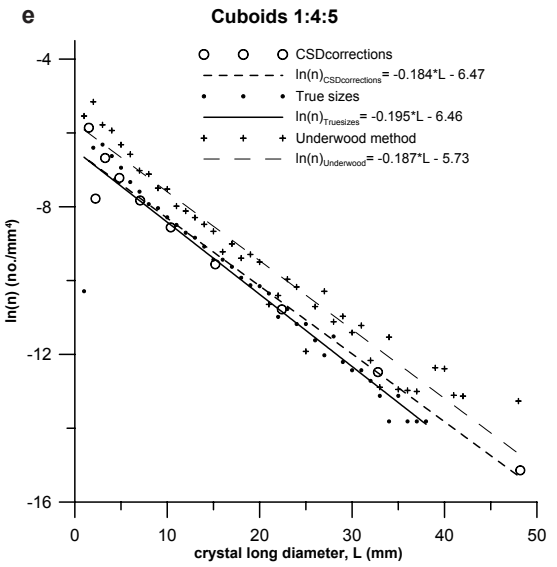

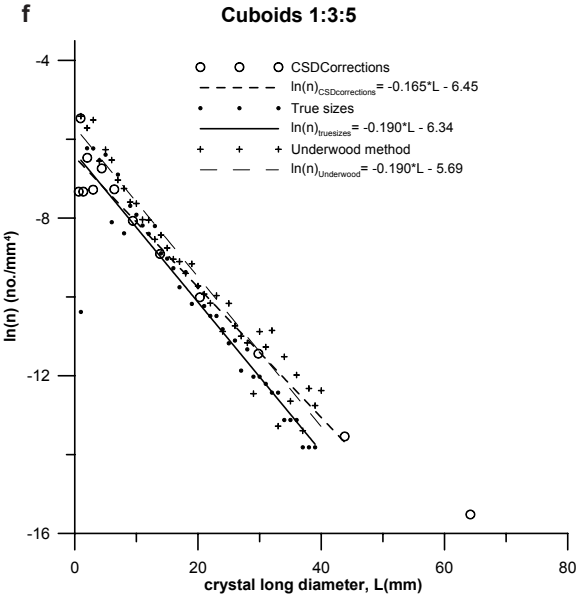

759

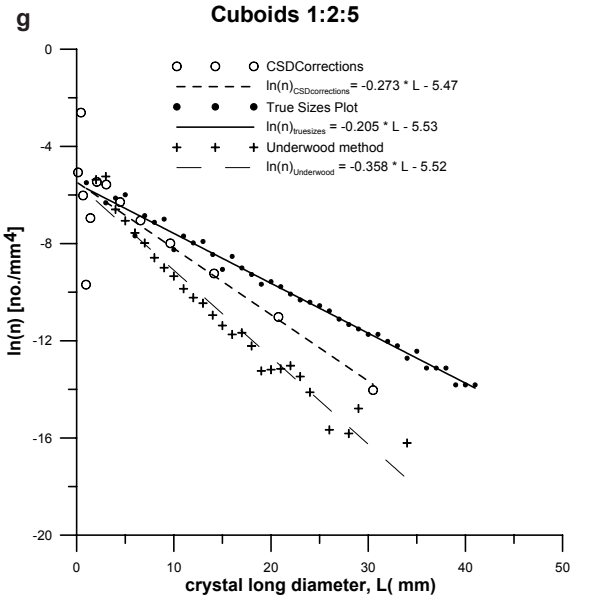

766

FIGURE 4.—*Continued*

larger overall population densities than those of the CSD if the true sizes. The Underwood method yielded curvilinear trends and in the prisms 1:1:3 smaller overall population densities. In the plates 1:5:5 (Fig. 4c) and 1:3:3 (Fig. 4d), CSDCorrections yielded slightly curvilinear trends and anomalously large crystal sizes. In the plates 1:3:3, CSDCorrections yielded a higher vertical intercept and slightly larger over all population densities, whereas the Underwood method yielded curvilinear trends. In the cuboids 1:4:5 (Fig. 4c) and 1:3:5 (Fig. 4f), CSDCorrections yielded curvilinear trends, and in the cuboids 1:3:5, it yielded an anomalously large crystal size that was off the trend; the Underwood method yielded pronounced curvilinear trends. The coefficients of determination (R^2) values for the results of CSDCorrections are given in the captions of Figure 4. The Spearman rank-order correlation coefficients, r_s, that do not depend on the normal distribution of the residuals from a straight line, are also given to better substantiate our results.

The percent slope difference between the CSD slope recovered with CSDCorrections and the true sizes slope for each data set are –2.9% for prisms 1:1:5, –3.4% for prisms 1:1:3, +12.3% for plates 1:5:5, –10.7% for plates 1:3:3, –5.6% for cuboids 1:4:5, and –13.2% for cuboids 1:3:5. A negative percent difference indicates the recovered CSD slope was less than the CSD slope for the true sizes. The closest slope agreement was found in the prisms, and the greatest difference was found in the cuboids. It should be noted that the Underwood method in some cases gave better slope agreements but the trends were markedly curvilinear.

The cuboids above belong in a class in which the length of the intermediate crystal diameter is closer to that of the long diameter, and in these cuboids, the measured intersection lengths appeared to correspond to the intermediate crystal diameters (Higgins 2000), and CSDs based on intersection lengths closely approximate the true sizes CSDs. However, cuboids (1:2:5) belong in an ill-behaved class. CSDCorrections yielded imperfect results using intersection widths (slope = –0.273, intercept = –5.47, Fig. 4g) but even worst results using intersection lengths (slope = –0.285, intercept = –7.16). The latter CSD is not shown since its population densities are significantly below the true size CSD (slope –0.205, intercept = –5.53). The results with this class of cuboids indicate that better stereological corrections need to be devised.

EVALUATING THE EFFECTS OF SLICE BOUNDARIES ON THE RECOVERED CSDS

The recovered CSDs shown in Figure 4 are based on all the crystals in each slice, including the crystals touching the slice boundaries. Each slice contained about 500 to 600 crystals and the boundary crystals were included comprise about 10%. The boundary crystals in the analyses of Figure 4 to test the accuracy of the stereological corrections for converting crystal area population densities in the slice to crystal volume population densities

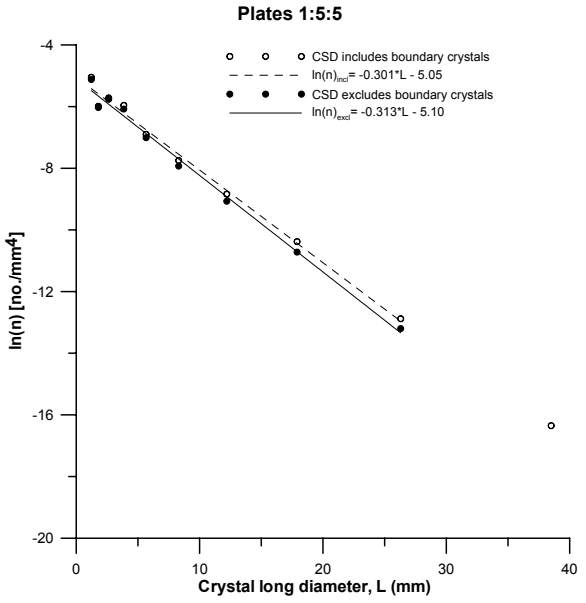

FIGURE 5. This figure for plates 1:5:5 is representative of all seven data sets. It compares the CSDs recovered with CSDCorrections on the data that include the crystals on the boundaries of the slices (dashed lines through open circles) and on the data subsets that exclude the boundary crystals (solid lines through closed circles). The steeper slopes of $CSD_{exclude}$ are believed to be due to the higher probability of the boundaries intersecting large crystals and avoiding small ones, hence excluding the boundary crystals would impose a negative bias in CSD slopes. The number of crystals in each data set are given in Table 1.

in the chamber. Another consideration was that the inclusion of the boundary crystals in the analyses maximized the number of crystals measured per slice. Even so, this number was low compared to rock thin sections, so at least three slices were needed for each data set. Furthermore, because most of the perimeter lengths of the boundary crystals were impingement contacts with other crystals, the growth environment of the boundary crystals appeared to be similar to that of the interior crystals.

To test if the boundary crystals in the slices had a significant affect on the recovered CSDs, subsets of the seven main data sets were formed that excluded the boundary crystals. Each subset contained about 10% fewer crystals than their respective main data sets (Table 1). The areas of the boundary crystals were subtracted from the total area of each slice to scale the remaining area population of crystals to the net slice area, and the CSDs were recovered on the subsets with CSDCorrections. The percent slope difference between $CSD_{include}$ and $CSD_{exclude}$ is 0.00% for the prisms 1:1:5; –5.10% for prisms 1:1:3; –3.99% for plates 1:5:5; –7.36% for plates 1:3:3; –1.63% for cuboids 1:4:5; –6.67% for cuboids 1:3:5; and –9.16% for cuboids 1:2:5. A negative value indicates that the slope of $CSD_{exclude}$ is steeper than the slope of $CSD_{include}$. Representative results are shown for the plates 1:5:5 in Figure 5. Note that the vertical intercepts of the two CSDs are in close agreement and that the steeper slope of $CSD_{exclude}$ is due largely to a reduction in the population densities in its larger crystal sizes. The reason for this can be seen in the microstructure of Figure 1b in which more large crystals than small ones touch the slice boundaries. This is a case of the intersection probability effect of the slice boundaries that are more likely to encounter large crystals and less likely to encounter small ones. Because the large crystals have lower population densities than the smaller ones in the main data sets, removal of the boundary crystals resulted in greater reduction in the population densities of the large crystal sizes in $CSD_{exclude}$ than in the small crystal sizes, as shown in Figure 5. Thus, we have chosen not to exclude the boundary crystals from the analyses in Figure 4, because any effects of the slice boundaries on crystal shapes is probably minor compared to the bias produced by excluding the boundary crystals.

DISCUSSION AND CONCLUSIONS

Our results suggest that computer modeling of crystallization can be used to better understand and constrain kinetic interpretations from crystal-size distributions in microstructures. The grain boundaries in our modeled microstructures are the result of dynamic competition for crystal growth space as in the models by Elliott et al. (1997). Slices through the modeled microstructures formed by prisms and plates show grain outlines similar to the intersection polygons through prisms and plates reported by Higgins (2000, Fig. 2). Similar grain outlines are commonly observed in thin sections of prismatic pyroxenes and platy plagioclases and micas. The modeled microstructures resemble the hypidiomorphic microstructures in some granites, although their monomineralic character would suggest better comparisons with non-cumulate pyroxenites, dunites, or anorthosites, or with clusters of pyroxene or plagioclase in diabases. The model results suggest that CSD information could be preserved in the microstructures of igneous rocks despite some modification of grain shapes and sizes by impingements and that more significant modification of the CSD information is more likely to be caused by secondary recrystallization processes than by the primary competition among growing crystals for space.

To generate the largest number of crystal shapes of the same type for each CSD database, our model dealt with development of microstructures composed of a single phase. Models that deal with more than one phase produce microstructures that are more realistic analogues for those in igneous rocks (e.g., Hersum and Marsh 2006). The growth of crystals by accretion of discrete volume units or unit cells is intended to simulate how real crystals grow by incorporating groups of atoms on to their surfaces. This also would provide a basis for recording the spatial compositions of minerals in future crystallization and recrystallization experiments. However, a problem with the method of growing crystals by accreting unit cells is that locating potential attachment sites requires increasingly more search time as crystals begin to impinge upon one another. Our computer runs that generated the microstructures took from three to four weeks. Larger scale models that implement crystal growth by unit cells would require algorithmic improvements and more computer power.

It would seem that the implementation of growth of stationary crystals in the model would be a severe restriction because crystals in a magma may be mobile depending on dynamic conditions. An early prototype program attempted to move 2-dimensional crystals that did not contain unit-cell structures (Amenta et al. 1992), but the algorithm proved too demanding in computer

time for moving 3-dimensional crystals with unit-cell structures. Although in real magmatic crystallization some crystal mobility may be likely during early stages of crystallization when crystals are few and magma viscosity is low, ultimately immobility would set in during late stages of crystallization as crystal contiguity and effective magma viscosity increase. The implication of the stationary growth model is that some crystals that do not have near neighbors may have unrestricted growth for longer periods during their growth history, but this situation is unlikely due to the random positioning of nuclei. Thus, we do not think that the model of stationary growth of crystals imposes a significant bias in our microstructures.

Our crystallization model has shown that the true CSDs in the microstructure are in close agreement with the ideal ones although the former exhibit more scatter of points relative to their regression lines. In recovering CSDs from 2-dimensional measurements of crystals in slices, our results confirm that the intersection widths are the best indicators of size for prisms and the intersection lengths are the best indicators for plates (Higgins 1994; Peterson 1996). CSDCorrections performed better than the Underwood method for approximating the true linear CSDs in the prisms, but produced slightly curvilinear CSDs in the plates and cuboids. The Underwood method produced CSDs with largest crystals in better agreement with the largest crystals in the true sizes, but the CSDs were strongly curvilinear. CSDCorrections gave mixed results with cuboids. For cuboids in which the intermediate diameter is closer to the long diameter, the intersection lengths were the best indicator for the intermediate crystal diameter; but for cuboids in which the intermediate diameter is closer to the short diameter neither the intersection width nor intersection length were a good indicator of crystal size.

ACKNOWLEDGMENTS

This research was supported by the Donors of the American Chemical Society Petroleum Research Fund grant PRF-39580-B2, and by the Division of Materials Research of the National Science Foundation REU grants DMR-0097449 and DMR-035377. I thank Bruce Marsh for suggesting the application of computer modeling for validating CSD recovery methods and for his encouragement and help, Michael Zieg for showing me how he measured real crystal-size distributions in his laboratory at Johns Hopkins; and Alex Mock, David Brakke, and Michael Higgins for their reviews and helpful criticisms of this manuscript.

REFERENCES CITED

Amenta, R.V. (2001) Three-dimensional computer modeling of fabric evolution in igneous rocks. Computers and Geosciences, 27, 477–483.

Amenta, R.V., Cooper, J.M., Bunting, R., and Romeo, C. (1992) Simulating fabric development in igneous rocks: A solution for modeling space competition among growing crystals. Computers and Geosciences, 18, 763–766.

Amenta, R.V., Holyoke, C.W., Myers Krohn, T.G., Bonder, M.J., and Leopold, M.C. (1997a) Undergraduate research in petrology approached through computer modeling of fabric evolution in igneous rocks. Journal of Geosciences Education, 45, 205–206.

Amenta, R.V., Bonder, M.J., Holyoke, C.W., Krohn, T.G.M., Leopold, M.C., and Miller C.C. (1997b) Computer modeling of microstructure evolution in polycrystalline materials and the formation of growth collision boundaries between crystals. Proceedings of the Ninth International Conference on High Temperature Materials Chemistry, 97, 397–404.

Amenta, R.V., Dadvar, P., Rodgers, R., and Ruotolo, G. (2002) Computer modeling of crystallization and crystal size distributions. Eos Transactions AGU, 83, Spring meeting supplement, abstract V51B-05.

Anderson, M.P., Grest, G.S., and Srolovitz, D.J. (1986) Microstructural dynamics of primary and secondary recrystallization. In D.J. Srolovitz, Ed., Computer Simulation of Microstructural Evolution, p. 77–93. Metallurgical Society, Warrendale, Pennsylvania.

Armienti, P., Pareschi, M.T., Innocenti, R., and Pompilio, M. (1994) Effects of magma storage and ascent on the kinetics of crystal growth: The case of the 1991–93 Mt. Etna eruption. Contributions to Mineralogy and Petrology, 115, 402–414.

Bindeman, I.N. (2003) Crystal sizes in evolving silicic magma chambers. Geology, 31, 367–370.

Cashman, K.V. and Marsh, B.D. (1988) Crystal size distribution (CSD) in rocks and the kinetics and dynamics of crystallization II. Makaopuhi lava lake. Contributions to Mineralogy and Petrology, 99, 292–305.

Castro, J.M., Cashman, K.V., and Manga, M. (2003) A technique for measuring 3D crystal-size distributions of prismatic microlites in obsidian. American Mineralogist, 88, 1230–1240.

Chayes, F. (1950) On the bias of grain-size measurements made in thin section. Journal of Geology, 58, 156–160.

Cheadle, M.J., Elliot, M.T., and McKenzie, D. (2004) Percolation threshold and permeability of crystallizing igneous rocks: The importance of textural equilibrium. Geology, 32, 757–760.

Elliott, M.T., Cheadle, M.J., and Jerram, D.A. (1997) On the identification of textural equilibrium in rocks using dihedral angle measurements. Geology, 25, 355–358.

Grest, G.S., Anderson, M.P., and Srolovitz, D.J. (1986) Computer simulation of microstructural dynamics. In D.J. Srolovitz, Ed., Computer Simulation of Microstructural Evolution, p. 21–32. Metallurgical Society, Warrendale, Pennsylvania.

Gualda, G.A.R. (2006) Crystal size distributions derived from 3D datasets: Sample size versus uncertainties. Journal of Petrology, 47, 1245–1254.

Hersum, T.G. and Marsh, B.D. (2002) On the link between crystallization kinetics and texture in basaltic rocks. EOS Transactions AGU, 83, Spring meeting supplement, abstract V51B-07.

——— (2006) Igneous microstructure from kinetic models of crystallization. Journal of Volcanology and Geothermal Research, 154, 34–47.

Higgins, M.D. (1994) Numerical modeling of crystal shapes in thin sections: Estimation of crystal habit and true sizes. American Mineralogist, 79, 113–119.

——— (1998) Origin of anorthosite by textural coarsening: Quantitative measurements of a natural sequence of textural development. Journal of Petrology, 39, 1307–1323.

——— (2000) Measurement of crystal size distributions. American Mineralogist, 85, 1105–1116.

——— (2006) Quantitative Textural Measurements in Igneous and Metamorphic Petrology, 270 p. Cambridge University Press, U.K.

Marsh, B.D. (1988) Crystal size distribution (CSD) in rocks and the kinetics and dynamics of crystallization I. Theory. Contributions to Mineralogy and Petrology, 99, 277–291.

——— (1998) On the interpretation of crystal size distributions in magmatic systems. Journal of Petrology, 39, 553–599.

——— (2002) Inherited correlation in crystal size distribution: Comment. Geology, 30, 284–285.

Mock, A. and Jerram, D.A. (2005) Crystal size distributions (CSD) in three dimensions: Insights from the 3D reconstruction of a highly porphyritic rhyolite. Journal of Petrology, 46, 1525–1541.

Mock, A., Jerram, D.A., and Breitkreutz, C. (2003) Using quantitative textural analysis to understand emplacement of shallow-level rhyolitic laccoliths—A case study from the Halle Volcanic Complex, Germany. Journal of Petrology, 44, 833–849.

Nasello, O.B. and Ceppi, E.A. (1986) Computer simulation of bidimensional grain boundary migration (II). In D.J. Srolovitz, Ed., Computer Simulation of Microstructural Evolution, p. 13–20. Metallurgical Society, Warrendale, Pennsylvania.

Ohser, J. and Muecklich, F. (2000) Statistical Analysis of Microstructures in Material Sciences, 381 p. Wiley, Chichester, U.K.

Pan, Y. (2001) Inherited correlation in crystal size distribution. Geology, 29, 227–230.

Peterson, T.D. (1996) A refined technique for measuring crystal size distributions in thin section. Contributions to Mineralogy and Petrology, 124, 395–405.

Randolph, A.D. and Larson, M.A. (1971) Theory of particulate processes, 251 p. Academic Press, New York.

Royet, J.P. (1991) Stereology: A method for analyzing images. Progress in Neurobiology, 37, 433–474.

Sahagian, D.I. and Proussevitch, A.A. (1998) 3D particle size distributions from 2D observations: Stereology for natural applications. Journal of Volcanology and Geothermal Research, 84, 173–196.

Saltikov, S.A. (1967) The determination of the size distribution of particles in an opaque material from measurements of the size distributions of their sections. In H. Elias, Ed., Proceedings of the Second International Congress of Stereology, 167–173. Springer-Verlag, Berlin.

Schaeben, H., van den Boogaart, G.K., Mock, A., and Breitkreuz, C. (2002) Inherited correlation in crystal size distribution: Comment. Geology, 30, 282–283.

Underwood, E.E. (1970) Quantitative Stereology, 274 p. Addison-Wesley, Massachusetts.

Zieg, M.J. and Marsh, B.D. (2002) Crystal size distribution and scaling laws in the quantification of igneous textures. Journal of Petrology, 43, 85–101.

MANUSCRIPT RECEIVED AUGUST 4, 2006
MANUSCRIPT ACCEPTED JULY 20, 2007
MANUSCRIPT HANDLED BY RAYMOND JONCKHEERE